Journal of Alloys and Compounds 770 (2019) 840–848

Contents lists available at ScienceDirect

Journal of Alloys and Compounds

journal homepage: http://www.elsevier.com/locate/jalcom

Evolution of microstructure and mechanical properties of Ti/TiB metal-matrix composite during isothermal multiaxial forging

M. Ozerov [a, *], M. Klimova [a], V. Sokolovsky [a], N. Stepanov [a], A. Popov [b], M. Boldin [b], S. Zherebtsov [a]

[a] Belgorod State University, Belgorod, Russia
[b] Lobachevsky State University of Nizhni Novgorod, Nizhni Novgorod, Russia

ARTICLE INFO

Article history:
Received 15 March 2018
Received in revised form
6 July 2018
Accepted 22 August 2018
Available online 25 August 2018

Keywords:
A. metal-matrix composites (MMCs)
B. precipitation
B. sintering
C. mechanical properties
C. microstructure
D. scanning electron microscopy

ABSTRACT

Mechanical behavior and microstructure evolution of a Ti/TiB metal-matrix composite during multiaxial forging (MAF) at 700 and 850 °C and a strain rate 10^{-3} s^{-1} were studied. The composite was produced via in-situ $3Ti + TiB_2 \rightarrow 2Ti+2TiB$ reaction during spark plasma sintering at 1000 °C. Mechanical behavior in terms of aggregated σ-Σε curves during MAF at both temperatures demonstrated a pronounced softening following by a steady-like flow stage. Microstructure evolution during MAF at both temperatures was associated with (i) dynamic recrystallization of the titanium matrix and the formation of dislocation-free areas of ~1 μm in diameter and (ii) shortening of TiB whiskers by a factor of ~3. MAF at 700 and 850 °C to cumulative strain ~5.2 resulted in a considerable increase in the low-temperature ductility without substantial loss in strength. Contributions of different strengthening mechanisms into the overall strength of the Ti/TiB metal–matrix composite were discussed.

1. Introduction

An attractive way to increase the strength-related properties (strength, hardness, wear resistance, etc.) in titanium and low-alloyed titanium alloys is embedding ceramic reinforcements into the Ti matrix [1,2]. Among many possible variants the use of titanium boride (TiB) is a very attractive option due to excellent thermodynamic stability, thermal expansion coefficients similar to the Ti matrix, a clean interface and excellent interface bonding between the TiB whiskers and the Ti matrix [3,4]. Ti/TiB metal-matrix composites (MMCs) can be obtained using different methods [3]. The spark plasma sintering (SPS) process through $3Ti + TiB_2 \rightarrow 2Ti+2TiB$ *in-situ* reaction seems to be one of the most promising ways as it can produce very fine structure thereby additionally promoting the strength-related properties [3–6].

Meanwhile, along with the increased strength, Ti/TiB MMCs demonstrate poor low-temperature ductility [3]. Mechanical properties of the MMCs can be improved by thermo-mechanical treatment. A considerable increase in both strength and ductility of a cast Ti/TiB MMC with 11 vol.% of TiB was achieved by so-called multiple isothermal 2-D forging which resulted in the formation of a microstructure with titanium boride whiskers aligned along the drawing axis [7,8]. However, in this earlier research, the thermo-mechanical treatment was carried out at rather high temperatures above the α↔β transition. Although titanium alloys show exceptionally high ductility in the β phase field, deformation in the α or α+β phase fields is usually more preferable due to lower energy consumption and finer attained microstructure [9].

Results obtained in Ref. [5] have shown that microstructure evolution of the Ti matrix in a MMC with 17% vol. of TiB during uniaxial compression in the interval of 500–1050°C was associated with different mechanisms depending on temperature: formation of a cell microstructure at 500 °C, continuous dynamic recrystallization at 700 °C and discontinuous dynamic recrystallization at temperatures ≥850 °C. It worth noting, however, that noticeable microstructure coarsening was observed after deformation in the β phase field [5]. The development of dynamic recrystallization suggests a possibility to carry out thermomechanical treatments at relatively low temperatures of 700–850 °C without fracture of the specimen. Uniaxial compressions also showed that the MMC was ductile enough at temperatures ≥700 °C [5,10]. Warm working of the Ti/TiB MMCs at temperatures much lower than the α↔β

* Corresponding author.
E-mail address: ozerov@bsu.edu.ru (M. Ozerov).

https://doi.org/10.1016/j.jallcom.2018.08.215
0925-8388/

transition can be quite attractive due to the possibility to produce a fine microstructure; however it is still unclear how structure and mechanical properties evolve during thermomechanical treatment at different temperatures and if it is possible to increase the low-temperature ductility. The latter is particularly important for finding the optimal processing window to improve the properties of MMCs.

In this paper, evolution of microstructure and mechanical properties of the 17 vol.% TiB reinforced titanium matrix composite produced by SPS at 1000 °C was studied during multiaxial forging at 700 and 850 °C.

2. Materials and procedure

Commercial Ti powders (wt.% of impurities: 0.07 N, 0.05C, 0.34H, 0.34 (Fe + Ni) and 0.1Si; the $\alpha \leftrightarrow \beta$ phase transition temperature was ~910 °C) and TiB_2 (wt.% of impurities: 0.04O, 0.04C, 0.02Fe) were used as the raw materials. In both cases, the particles had an irregular shape; the average particles size of the Ti and TiB_2 powders were ~25 and ~4 μm, respectively (Fig. 1). A mixture of 90 wt. % Ti and 10 wt. % TiB_2 (which yields ~17 vol.% of TiB during the reaction of $3Ti + TiB_2 \rightarrow 2Ti+2TiB$ [11]) was prepared using a Retsch RS 200 vibrating cup mill for 1 h in ethanol at the milling rotation speed of 700 rpm. The amount of TiB_2 was selected to attain a high strength in combination with some (very low though) ductility [3].

The Ti/TiB metal-matrix composite was produced using the SPS process under vacuum on a Thermal Technology SPS 10-3 machine at 1000 °C and 40 MPa for 15 min. Specimens measuring 15 mm in height and 19 mm in diameter were obtained. The residual porosity of the specimens was determined using both metallographic analysis in various cross-sections and hydrostatic weighing on a Porotech 3.1 Automated Standard Porosimeter.

Prismatic samples measured $16 \times 14 \times 12\ mm^3$ were cut from the sintered Ti/TiB preforms using an electric-discharge machine. The specimens were subjected to multiaxial forging (MAF) which comprised successive compressions of a sample along three orthogonal directions (this method is also known as “abc” deformation [12]). Using this method a very high cumulative strain level can be attained. In addition, the stress-strain curve of each deformation step can be recorded allowing the analysis of mechanical behavior of the specimen during large straining; to this end a prismatic shape was restored to the samples by electric-discharge machining the curved faces prior to each rotation. The initial strain rate and the true strain per deformation step were $10^{-3}\ s^{-1}$ and ~0.5, respectively. Compressions were performed on an Instron 300LX testing machine in the laboratory air at 700 or 850 °C (hereafter these conditions will be designated as MAF700 and MAF850, respectively). The stress-strain curves were recorded for each step. Ten compressions in total were made at each temperature (the cumulative strain $\Sigma\varepsilon \approx 5.2$). Variations in the specimens density during MAF was measured by hydrostatic weighing.

An ARL X'TRA powder diffractometer with CuKα radiation was used for XRD measurement. The diffraction lines were recorded for the interval of $2\theta = 15–80°$ with a step of 0.02°. The observed diffraction peaks were corrected with respect to $CuK\alpha_1$ or $CuK\alpha_2$ radiations and fitted with Pseudo-Voigt function. The instrumental line broadening was evaluated by using Si characteristics as the standard reference material. Crystallite size and lattice strain were estimated from the broadening of XRD peaks by using the Williamson-Hall method. Quantitative phase analysis was performed using the Rietveld method [13] with PowderCell software.

A Quanta 600 FEG field-emission-gun scanning-electron microscope (FEG SEM) and a JEOL JEM-2100 transmission electron microscope (TEM) were used for microstructure examination. All microstructure observations were focused on the central (most highly deformed) region of the compression specimens. For SEM observations, the specimens were mechanically polished in water with different SiC papers and colloidal silica suspension (the final size of the Al_2O_3 abrasive was 0.05 μm) and then etched with the Kroll's reagent (95% H_2O, 3% HNO_3, 2% HF) to reveal the TiB whiskers. Thin-foil specimens for TEM characterization were prepared by mechanical thinning followed by electropolishing on a twin-jet TENUPOL-5 at 29 V and at −35 °C using an electrolyte containing 60 ml perchloric acid, 600 ml methanol and 360 ml butanol.

The linear intercept method (the lengths of intercepts along or across each particle) was used to determine the average apparent length or diameter of the TiB whiskers. For this purpose, a total area of approximately $1150\ \mu m^2$ was examined for each condition.

The dislocation density was determined by counting the individual dislocations within the grains/subgrains using at least six arbitrarily selected TEM images for each sample according to a standard procedure described in Ref. [14].

Tensile tests were conducted at temperatures of 300 °C, 400 °C and 500 °C and an initial strain rate of $10^{-3}s^{-1}$. Dog-bone shaped tensile samples had the gauge measured 4 mm length and $3 \times 1.5\ mm^2$ cross-section. The specimens were carefully mechanically polished. Elongation to fracture was determined by measurements of spacing between marks designating the gauge length before and after the test. Compression of rectangular specimens measured $7 \times 7 \times 10\ mm^3$ was carried out at room temperature using an Instron 300LX test machine. The initial strain rate was $10^{-3}\ s^{-1}$. Two samples of each condition were tested at each temperature (both in tension and compression) to obtain representative stress-strain curves.

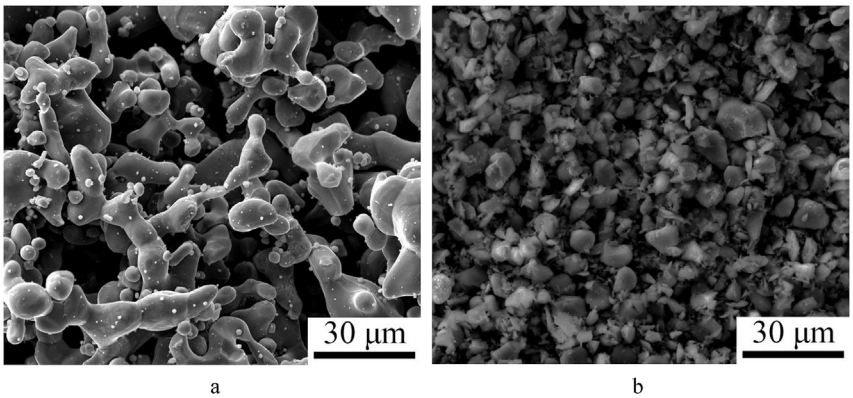

Fig. 1. SEM images of Ti (a) and TiB_2 (b) particles used for the Ti/TiB composites production.

3. Results

3.1. Characterization of the initial condition

In the initial condition the microstructure of the Ti/TiB MMC produced using SPS at 1000 °C consisted of TiB whiskers heterogeneously distributed within the Ti matrix (Fig. 2a). The diameter of the TiB whiskers varied in a wide interval from tens to few hundred nanometers. The average diameter of the TiB whiskers in the initial condition was found to be 63 ± 35 nm. The volume fraction of unreacted TiB_2 particles was~2%. The residual porosity was ~0.5%.

TEM examination also revealed TiB whiskers heterogeneously distributed in the Ti matrix (Fig. 2b). In the majority of the microstructure a very high dislocation density was observed most probably due to a large number of TiB particles. The TiB whiskers had an irregular hexagonal shape (insert in 2b) with sides formed by the (100), (101) and (10$\bar{1}$) planes [15]. Many stacking faults were observed in the (100) plane of the TiB whisker. Due to the presence of an orientation relationship (OR) between the TiB particles and the Ti matrix (which is usually described as $(10\bar{1}0)_\alpha//(100)_{TiB}$ and $[01\bar{1}0]_\alpha//[0\bar{1}1]_{TiB}$ [4]), the interphase Ti/TiB boundaries are very clear without noticeable internal stresses. Some deviation from the "classical" OR can occur in case of sintering above the α/β phase transformation temperature, as it was discussed in details earlier [15]. However in the present case this factor does not have any influence on properties of the MMC since all the specimens were produced under the same conditions.

X-ray analysis showed (Fig. 3) that the Ti/TiB MMC consisted of α-Ti, TiB_2 with a hexagonal lattice, and TiB with an orthorhombic lattice. The determined volume fractions of the phases were 79.3 ± 4.5% Ti, 18.7 ± 2.0% TiB and 2.0 ± 0.5% TiB_2.

3.2. Evolution of microstructure and mechanical properties during MAF

XRD patterns obtained after MAF at both temperatures (Fig. 3) did not show any marked difference in the phase composition of the Ti/TiB MMC. However, the diffraction maximums from α-Ti were slightly broader in the deformed conditions. Evaluation of the full width at the half maximum of the relatively well-defined (0002) and (10$\bar{1}$1) peaks revealed some increase after MAF at 850 °C in comparison with the corresponding values for both the as-sintered and MAF700 conditions. The peak broadening can be associated with a greater dislocation density and greater residual stresses. Indeed, the dislocation density in the MAF850 condition was estimated as ~$1.2 \times 10^{16} m^{-2}$ while these values for other two conditions (as-sintered and MAF700) were found to be $(0.6–0.7) \times 10^{16} m^{-2}$.

True stress-true strain curves obtained during multi-axial isothermal forging at 700 or 850 °C are shown in Fig. 4. At each temperature the stress-strain curves during the first compression exhibited an initial hardening transient, a peak flow stress, and then pronounced flow softening. Further steps of MAF at 700 °C were associated with a continuous increase of the flow stress during compression. However at 850 °C the stress-strain curves after the sixth step demonstrated a steady-state-like behavior. A noticeable difference between the flow stresses at the end of each step and the yield stress of the next step was observed at both temperatures. It should be noted also, that the flow stress at the end of each step did not change noticeably at 700 °C while at 850 °C the flow stress at the end of each step tended to decrease. In general, the flow stress was ~2.5 times higher at 700 °C than that at 850 °C.

The microstructure of the Ti/TiB MMC changed considerably as a result of MAF. The main difference was associated with the appearance of a large number of debris of TiB in the microstructure of strained conditions (Fig. 5). It should be noted that any noticeable effect of deformation temperature (700 or 850 °C) or the number of steps (5 or 10) on the microstructures after MAF was not found via SEM.

Quantitative analysis showed a similar effect of the multiaxial deformation at 700 or 850 °C on the diameter and apparent length of the TiB whiskers. The diameter of the whiskers (63 ± 35 nm in the as-sintered condition) did not noticeably change during MAF at both temperatures. The apparent length of whiskers at both deformation temperatures decreased considerably, by a factor of ~3, after the first step of MAF and then either remained almost unchanged during deformation at 850 °C or tended to decrease slowly at 700 °C (Fig. 6). The length-to-diameter aspect ratio of TiB whiskers approached the stable value of ~10 at the initial stages of deformation and had not changed further.

It is worth noting that the density of the specimens after MAF varied within a very narrow interval ($\Delta = \pm 0.015$ g/cm^3) at both temperatures suggesting that internal microcracks do form in the MMCs microstructure during deformation.

Meanwhile TEM analysis evidently showed an influence of the deformation temperature and strain on the structure of the Ti matrix of the composite. Deformation at 700 °C to e = 2.6 (5 steps) resulted in the formation of separate areas (0.5–1 μm in diameter) with a much lower dislocation density compared with the neighboring fields (Fig. 7a). The estimated dislocation density in these areas was ~$2 \times 10^{12} m^{-2}$. Boundaries of those dislocation-free areas were rather sinuous and unclear. The size and volume fraction of

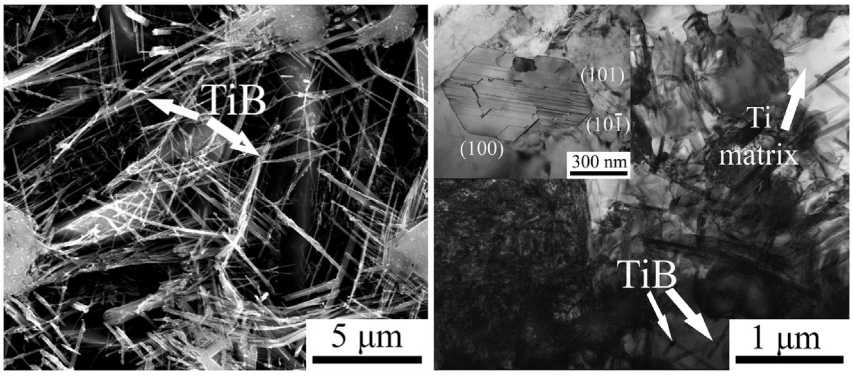

Fig. 2. SEM (a) and bright-field TEM (b) microstructure of the Ti/TiB MMC; a cross-section of a TiB whisker is shown in the insert in Fig. 2b.

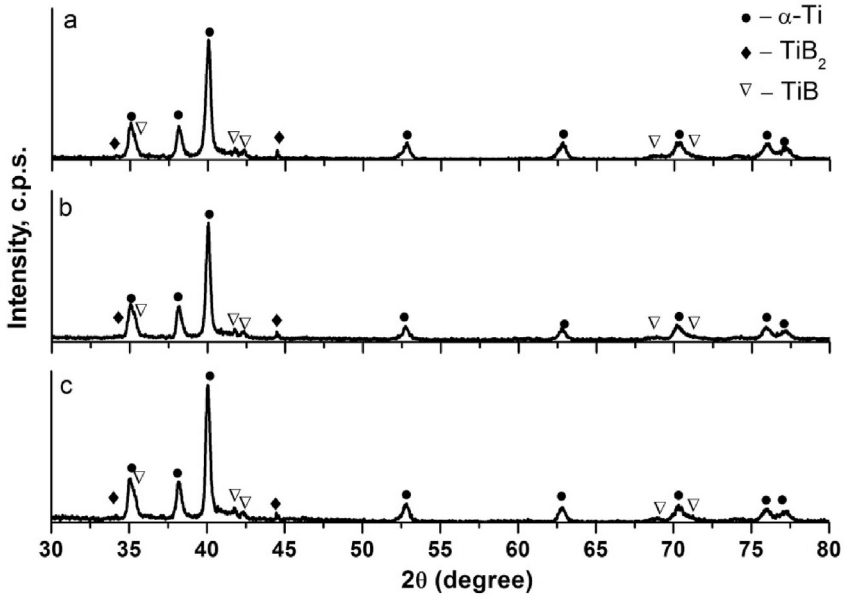

Fig. 3. XRD patterns of the Ti/TiB MMC in the as-sintered condition (a) and after MAF to e = 5.2 (10 steps) at 700 °C (b) or 850 °C (c).

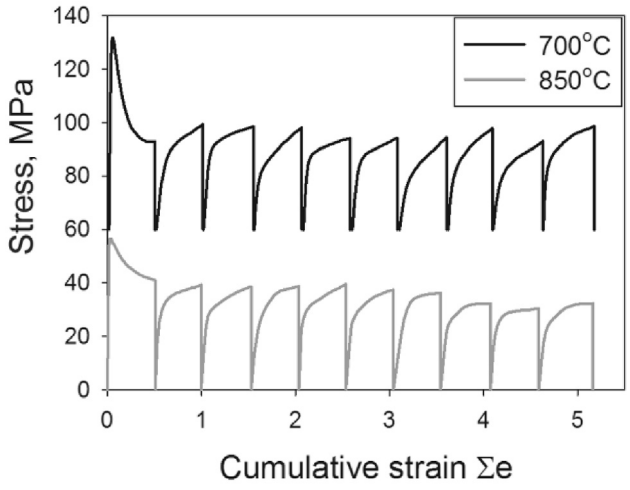

Fig. 4. Cumulative true stress-true strain curves obtained during multi-axial isothermal forging at 700 °C or 800 °C of the Ti/TiB MMC sintered at 1000 °C.

the recovered/recrystallized areas increased with strain increasing to e = 5.2 (10 steps) during MAF at 700 °C (Fig. 7b).

At a higher deformation temperature (850 °C) the formation of a partially recrystallized microstructure was also observed (Fig. 8a). The size of the recrystallized grains (some of them had well-defined boundaries) was found to be 1–1.5 μm. Similarly to the lower temperature, the size and the volume fraction of the recrystallized/recovered areas increased with strain during MAF at 850 °C (Fig. 8b). The dislocation density in the recrystallized areas was almost the same as that at the lower temperature. At both temperatures the development of recovery or recrystallization was more evident in the areas of the Ti matrix with a relatively low density of the TiB whiskers. The greater density of the TiB particles most likely hindered grain boundary movement thereby preserving deformed microstructure. However even in the areas with a high density of TiB the microstructure seemed more recrystallized at the final stages of MAF (Figs. 7b and 8b vs. 7a, 8a).

3.3. Brittle-to-ductile transition in a Ti-TiB metal-matrix composite after MAF

One of the most interesting findings of this work was associated with a notable decrease in the brittle-to-ductile transition temperature of the Ti/TiB composite due to multiaxial forging. Usually tensile testing is used for determination of main mechanical characteristics of metallic materials (i.e. yield stress, tensile strength, total elongation). However, because of the limited ductility of both as-sintered and forged specimens at room temperature, compression test having a “softer” deformation scheme was carried out. At higher temperatures (300–500 °C, where the ductility of the MMCs was expected to be high enough) tensile tests were conducted.

Mechanical behavior of the MMCs obtained in compression at room temperature (Fig. 9a) or in tension at 300–500 °C (Fig. 9b and c) showed a considerable improvement of the specimens ductility after MAF. The samples of the MMC after MAF at 700 and 850 °C to e = 5.2 (10 steps) showed noticeable compression ductility (~2–3%) at room temperature in contrast to the as-sintered specimen which demonstrates the ductility close to zero. Note that the temperature of MAF had no noticeable effect on the compression mechanical behavior of the composite at room temperature. The ultimate compression strength of the forged at 700 and 850 °C and as-sintered specimens were found to be quite similar (1960, 1970 and 2210 MPa, respectively).

The tensile stress-strain curves obtained at 300–500 °C of the specimens in the as-sintered condition or after MAF to e = 5.2 (10 steps) at 700 or 850 °C are shown in Fig. 9b and c. The tensile properties of the MMC in different conditions are summarized in Table 1. During tensile testing the samples of the MMC after MAF at 700 °C showed the ductility of ~4% at 300 °C (Fig. 9b). Meanwhile in the as-sintered condition the specimen of MMC even at 400 °C fractured just after the elastic region. Some tensile elongation of the as-sintered composite was recorded at 500 °C; it is interesting to note that very similar mechanical behavior was demonstrated by the MAF700 condition at 400 °C (Fig. 9b) thereby indicating a

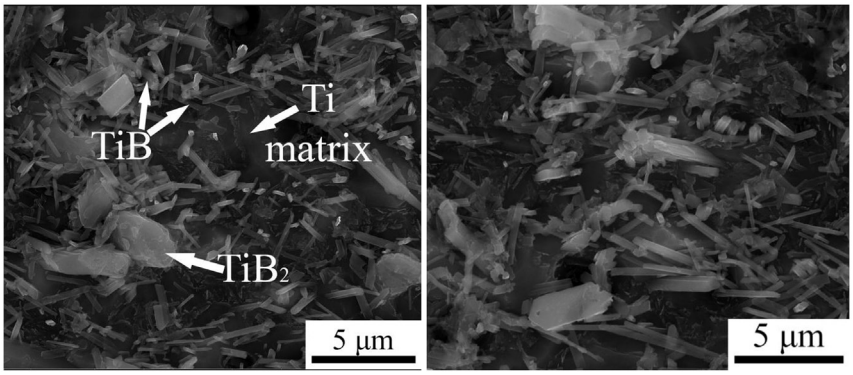

Fig. 5. SEM image of Ti/TiB composite subjected to 10 steps of MAF at 700 °C (a) or 850 °C (b).

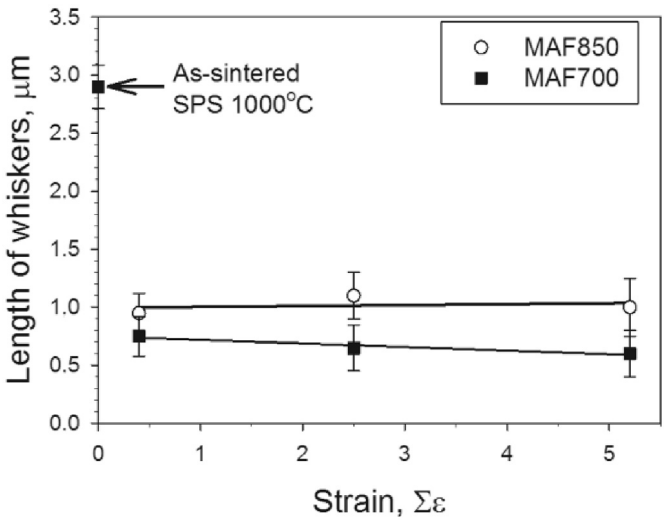

Fig. 6. Apparent length of TiB whiskers in Ti/TiB MMC during MAF at 700 or 850 °C.

considerable increase in the ductility and some decrease in the strength of the MMCs as a result of MAF. One can see that MAF at 700 °C resulted in somewhat higher ductility and lower strength in comparison with MAF850 specimens, especially at the higher testing temperature. At 300 °C the difference in the tensile elongation was found to be ~2%, while at 400 °C the difference was ~6%. The strength of the MAF700 specimens at 400 °C was ~60 MPa lower than that of MAF850; at 300 °C the strength was almost same, however.

SEM images of fracture surfaces of the Ti/TiB MMC samples in the as-sintered condition (Fig. 10a) or after MAF at 700 °C to e = 5.2 (Fig. 10b) tensile tested at 400 °C showed an obvious difference in the fracture mechanisms. The as-sintered condition demonstrated a brittle fracture mode corresponding to intergranular fracture (Fig. 10a). After MAF at 700 °C the specimen exhibited an obvious ductile fracture surface with the formation of typical dimples which size corresponded with the size (~1–1.5 μm) of the recrystallized areas (Fig. 10b). These observations also confirmed the suggestion about the shift of the ductile-to-brittle transition in Ti/TiB MMC by ~100 °C as a result of MAF.

4. Discussion

The results obtained in the current study shows a possibility to increase considerably the room and elevated temperature ductility without substantial loss in the strength of the Ti/TiB MMCs using multiaxial isothermal forging at 700 or 850 °C to ε = 5.2. The observed improvement of mechanical properties is most likely associated with the microstructure developed during MAF at both temperatures.

One of the most obvious effects of plastic deformation at elevated temperatures on the microstructure of Ti/TiB MMC was a considerable (by ~3 times) decrease in the length of the TiB whiskers. This change occurred in the very beginning of MAF (Fig. 6)

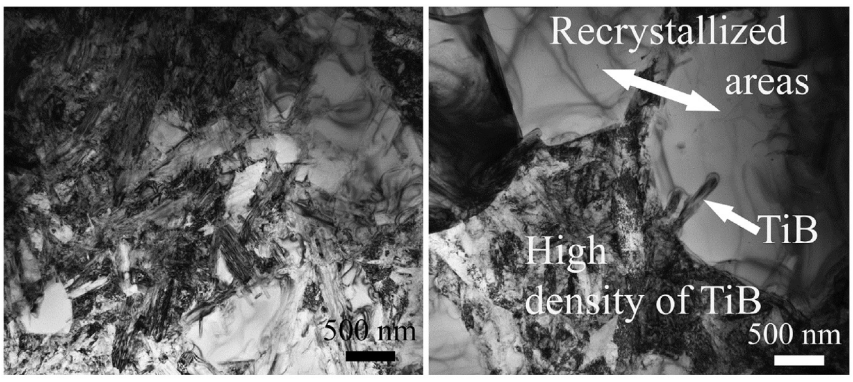

Fig. 7. TEM bright-field images of Ti/TiB MMC subjected to MAF at 700 °C to e = 2.6 (5 steps) (a) or e = 5.2 (10 steps) (b).

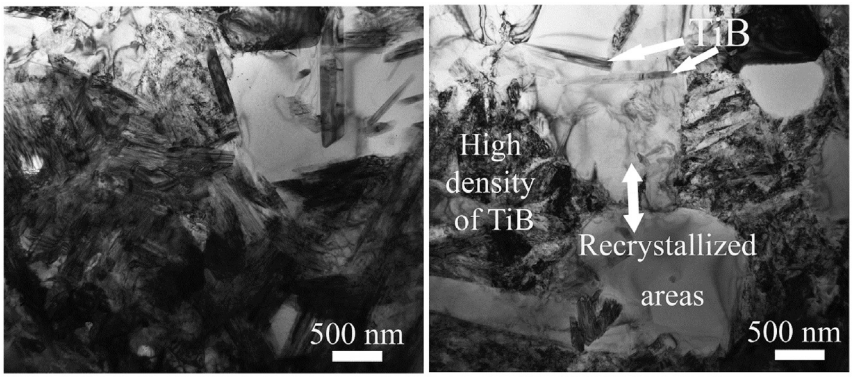

Fig. 8. TEM bright-field images of Ti/TiB MMC subjected to MAF at 850 °C to e = 2.5 (5 steps) (a) or e = 5.2 (10 steps) (b).

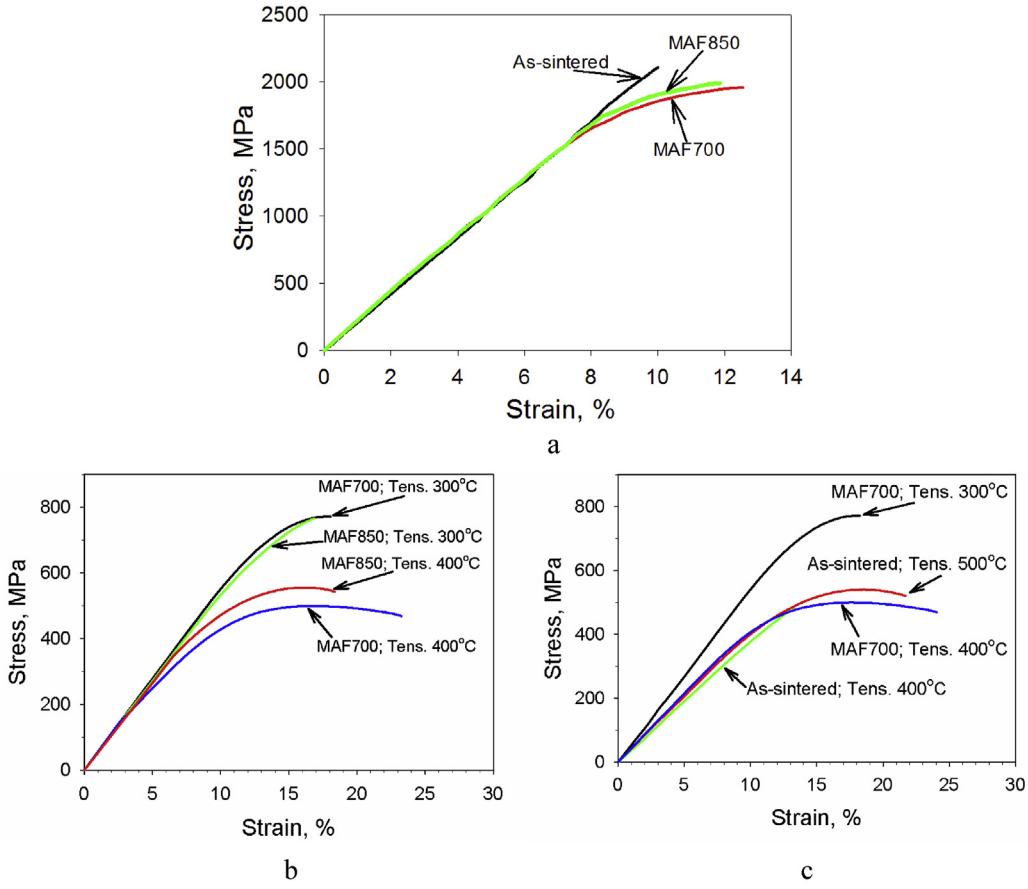

Fig. 9. Stress-strain curves of Ti/TiB MMC in different conditions tested in compression at room temperature (a) or in tension at 300–500 °C (b, c).

Table 1
Tensile mechanical properties of the Ti/TiB MMC in different conditions.

Condition	Testing temperature	σ_B	$\sigma_{0.2}$	δ, %
Initial	400 °C	483	420	0.5
	500 °C	540	410	9
MAF 700 °C	300 °C	770	610	4
	400 °C	500	363	14
MAF 850 °C	300 °C	765	575	2
	400 °C	560	390	8

causing, most likely, the corresponding decrease in the flow stress after the first compression (Fig. 4). Since the apparent length of the TiB whiskers did not decrease noticeably with further strain even at the lowest temperature (700 °C), a stable aspect ratio of ~10 at both deformation temperatures was achieved. The aspect ratio of the TiB (rather than the diameter) is considered to be the main factor that influences the mechanical properties of the MMCs [16]; therefore a stable length/diameter ratio after MAF can result in the observed improvement of ductility in comparison with the as-sintered

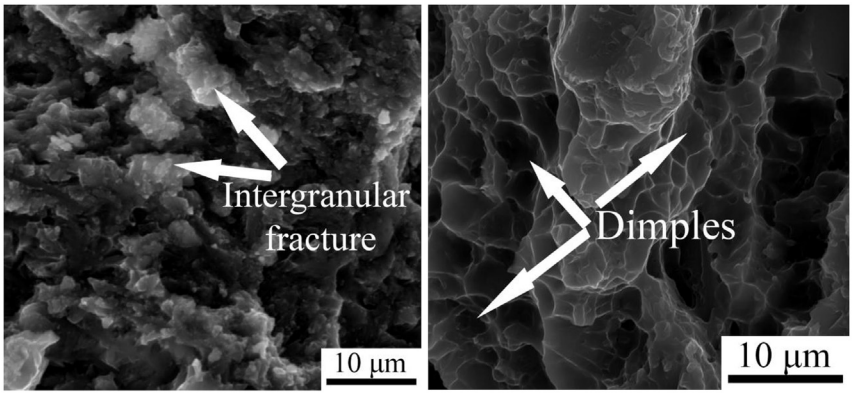

Fig. 10. Fracture surfaces of tensile tested specimens at 400 °C in the as-sintered condition (a) or after MAF at 700 °C to e = 5.2 (10 steps) (b); SEM images.

condition (Fig. 9). It worth noting that a similar mechanical behavior during multiaxial forging and a noticeable improvement of mechanical properties due to the transformation of a lamellar structure into a globular one was also observed in two-phase α/β titanium alloys e.g. Ref. [17]. Although deformation characteristics of the TiB whiskers in the MMC and the α or β phases in two-phase titanium alloys are completely different, the effect of shortening of the reinforcing phase has rather similar effects. In addition some decrease in the flow stress at both temperatures can be associated with the rotation of structural constituents towards "softer" orientations with low Taylor factors [18,19].

Some difference in the mechanical behavior of the MMC during MAF at 700 or 850 °C and in the resulting mechanical properties of the specimens after MAF can also be ascribed to different processes developed in the Ti matrix of the composite. As it was shown earlier [5] microstructure evolution of the Ti matrix at these temperatures can be associated with continuous (700 °C) or discontinuous (≥850 °C) dynamic recrystallization. Both types of the restoration processes are associated with the formation of new dislocation-free grains (Figs. 7 and 8) and have a characteristic type of the aggregated mechanical behavior with a steady-like flow stage at 700 °C or a slight decrease in the flow stress at 850 °C during MAF (Fig. 4). An intensive decrease in the flow stress occurred during the first step of MAF is often observed during discontinuous dynamic recrystallization [20], however it is less typical of continuous dynamic recrystallization (cDRX). Nevertheless the appearance of a drastic drop in the flow stress associated with the development of cDRX was earlier observed during warm compression of a magnesium alloy AZ31 [21] or after the first step of MAF of an aluminum alloy [22].

Meanwhile it should be noted, that the joint analysis of microstructure and mechanical properties of the specimens deformed at 700 or 850 °C shows rather surprising results. According to the results of X-ray analysis, MAF at the higher temperature (850 °C) led to a higher dislocation density in comparison with that after MAF700. This finding is in agreement with the mechanical behavior of the MMC after MAF at 700 and 850 °C: the latter condition showed slightly less ductility and higher strength at 400 °C (limited ductility of both conditions prevent a correct comparison at 300 °C).

In contrast to the integral data obtained by X-ray analysis (the XRD data were collected from an area of ~1 cm^2), a local estimate of the dislocation density in the recrystallizes grains obtained by TEM showed quite similar values for both deformation temperatures. Since the size of the recrystallized grains is also quite similar for both deformation temperatures, it can be suggested that the observed difference in the mechanical properties is most likely associated with the microstructure in the areas with a high density of the TiB whiskers and, respectively, with a high dislocation density. The lower dislocation density after MAF700 in those areas can therefore be related to the more intensive shortening of the TiB whiskers (Fig. 6). Shorter TiB whiskers increase the possibility to overcome the obstacle by dislocations thereby making easier their redistribution and decreasing the overall dislocation density. It should be noted that the average length of TiB after MAF showed in Fig. 6 can be overrated because very small debris of TiB cannot be distinguished by SEM. The presence of the very small TiB particles not only shifts the average length of TiB towards a smaller size but most probably increases the scatter in the average length of TiB and thereby increases the difference in this parameter between MAF700 and MAF850. All these findings support the suggestion about the easier development of relaxation processes during MAF700.

The combination of the recrystallized Ti grains and the nano-sized strengthening TiB whiskers provides a very good balance of strength and ductility; the latter exceeds the corresponding properties of the as-sintered material (at room temperature – in compression (Fig. 9a); at elevated temperatures – in tension (Fig. 9c)). This approach (formation of a nanocrystalline or ultrafine-grained structure with the insert of micrometer-sized recrystallized grains) being suggested to improve the poor ductility of nanocrystalline materials at low temperatures [23] was successfully realized with respect to ultrafine-grained Ti-6Al-4V alloy produced by warm MAF [24]. Some increase in ductility after drawing (2D forging) in the β-field of a Ti/TiB MMC was also reported in Refs. [7,8]. However in this latter case better mechanical properties in the drawing direction were ascribed to the formation of a fiber microstructure with the TiB whiskers aligned along the deformation axis.

The contributions of the most relevant hardening mechanisms in the overall composite strength can be expressed as [25]:

$$\sigma\Sigma = \sigma_0 + \sigma_{SS} + \sigma_\rho + \sigma_{H-P} + \sigma_{L-T} + \sigma_{TiB(OR)} \quad (1)$$

where σ_0 is the friction stress, σ_{SS} is solid solution strengthening, σ_ρ is dislocation substructure strengthening, σ_{H-P} is Hall-Petch strengthening, σ_{L-T} is hardening due to a load transfer from the Ti matrix to TiB by an interfacial shear stress, $\sigma_{TiB(OR)}$ is precipitation hardening by the debris of the TiB whiskers (Orowan mechanism).

The total solid solution strengthening effect due to the interstitial C, O and N atoms in titanium was found to be 160 MPa according to Ref. [26]. Some contamination of the Ti powder can also occur during the Ti/TiB_2 mixture preparation, however a possible effect was neglected in this calculation. Together with the friction

Table 2
Contribution of various strengthening mechanisms into the overall strength of Ti/TiB MMC in different conditions.

Condition	Contribution of various strengthening mechanisms, MPa					Compression strength, MPa	Predicted strength, MPa
	σ_0	σ_ρ	σ_{H-P}	σ_{L-T}	$\sigma_{TiB(Or)}$		
MAF700	496	133	110	220	856	1960	1815
MAF850		189		340	750	1970	1885

stress for pure Ti (336 MPa [27]), the value of σ_0 was accepted to be 496 MPa. The solubility of boron in titanium is very low (<0.001 at %) [28] therefore the effect of boron atoms on strengthening was neglected.

The dislocation substructure hardening σ_ρ can be expressed as:

$$\sigma_\rho = M\alpha Gb\sqrt{\rho} \quad (2)$$

where M is the average Taylor factor, α is a constant, G is the shear modulus, b is the Burgers vector and ρ is the dislocation density (0.6×10^{16}m^{-2} for MAF700 and 1.26×10^{16}m^{-2} for MAF850). The values of M and α were taken equal to 3 and 0.2, respectively [29]. The Burgers vector $b = 2.9 \times 10^{-10}$ m for the titanium matrix were taken from Ref. [27]. The value of the shear stress $G = 98$ GPa for Ti/TiB MMCs was calculated using expression $G = E/2(1+\nu)$, where $E = 130$ GPa is the Young's moduli and $\nu = 0.32$ is the Poisson coefficient [3]. The volume fractions of Ti and TiB determined using X-ray analysis were 0.786 and 0.2, respectively. The contributions of the dislocation substructure strengthening were found to be 133 MPa and 189 MPa for MAF700 and MAF850, respectively.

The Hall-Petch hardening contribution can hardly be evaluated in the present case because of the lack of a grain structure. However earlier calculations estimated the contribution of Hall-Petch hardening as 8–10% of the overall MMCs strength [30,31]. In our case $\sigma_{H\text{-}P}$ was accepted to be 110 MPa.

The load transfer strengthening effect was calculated as [25]:

$$\sigma_{L-T} = \left[\left\{V_{TiB}\left(\frac{S+2}{2}\right) + V_{Ti}\right\} - 1\right] \quad (3)$$

where V_{TiB} and V_{Ti} are the volume fractions of the corresponding phases, S is the aspect ratio of TiB whiskers. The contributions of the load transfer strengthening were found to be 220 MPa and 340 MPa for MAF700 and MAF850, respectively.

The precipitation hardening $\sigma_{TiB(OR)}$ (per the Orowan mechanism) can be calculated using formula [30]:

$$\sigma_{TiB(Or)} = \frac{MGb}{2.36\pi} ln\left(\frac{0.57DS^{\frac{1}{3}}}{b}\right) \frac{1}{\left(0.92V_{TiB}{}^{-\frac{1}{3}} - 1.14\right)DS^{\frac{1}{3}}} \quad (4)$$

where D is the diameter of TiB whiskers. The contributions of precipitation hardening were found to be 856 MPa and 750 MPa, respectively for MAF700 and MAF850.

In the case of composite materials, some contribution to the total strength can also be expected from Ref. [25] prismatic punching of dislocations at the Ti/TiB interface due to thermal mismatch between Ti and TiB. However due to the very small difference in the coefficients of thermal expansions the effect of prismatic punching of dislocations at Ti/TiB interface on strength was too small to mention.

The values of all strengthening mechanism are tabulated in Table 2. Note that in the present analysis the effect of the remnant TiB_2 particles was neglected; it is expected to be insignificant because of their big size and the small fraction. The predicted value of strength calculated by summing the contribution of all the above-mentioned hardening mechanisms gave 1815 and 1885 MPa for MAF700 and MAF850, respectively, which is reasonably close to the ultimate compression strength values of the Ti/TiB composite at room temperature (Fig. 9a, Table 2).

It should be noted that the precipitation hardening by the debris of the TiB whiskers makes the most appreciable contribution - 750 or 856 MPa (~50%) among all other strengthening mechanisms. A close value of the Orowan strengthening contribution was obtained in a Ti/TiB metal–matrix composite after high-pressure torsion at 400 °C [31]. Therefore, the properties of MMCs are most probably associated with the morphology and distribution of reinforcements rather than with the properties of the matrix and it can be suggested, that deformation treatments of MMCs have a good potential for improvement of mechanical properties of MMCs and therefore deserves further investigation.

5. Conclusions

Mechanical behavior and microstructural response of a Ti/TiB metal-matrix composite produced by spark plasma sintering (SPS) at 1000 °C using a Ti-10 wt.%TiB_2 powder mixture to multiaxial isothermal forging at 700 or 850°C and a strain rate 10^{-3} s^{-1} were studied. The following conclusions can be drawn from this work:

1) Mechanical behavior during MAF can be described by an aggregated σ-Σε curves which demonstrated a pronounced softening following by a steady-like state flow at 700 °C or slight softening at 850 °C. The observed mechanical behavior can be associated with the formation of a stable aspect ratio of ~10 of the TiB whiskers during MAF and development of dynamic recrystallization.
2) Microstructure evolution of the MMC was associated with discontinuous dynamic recrystallization during MAF at 850 °C or continuous dynamic recrystallization during forging at 700 °C. MAF at both temperatures resulted in the formation of a heterogeneous microstructure with i) dislocation-free recrystallized areas of 1–1.5 μm and ii) areas with high density of TiB and high dislocation density. Shortening of TiB whiskers by a factor of ~3 also occurred at both temperatures.
3) MAF at 700 and 850 °C to cumulative strain ~5.2 resulted in a considerable increase in low-temperature tensile ductility without substantial loss in strength. For instance, elongation of only 0.5% was obtained in the as-sintered specimen during a tensile test at 400 °C, whereas specimens after MAF demonstrated tensile elongation of 8–14% at the same temperature. Compression tests at room temperature showed nearly zero ductility in the as-sintered specimen, whereas specimens after MAF850 demonstrated at this temperature ~3% ductility.
4) Analysis of different strengthening mechanisms into the overall strength of the Ti/TiB metal–matrix composite shows that the main contribution (~50%) can mostly be ascribed to precipitation hardening by the TiB whiskers debris.

Acknowledgements

The work was supported by the Russian Science Foundation under Grant № 15-19-00165. The authors are also grateful to Joint

Research Center “Materials and Technologies”, Belgorod State University, for the assistance with instrumental analysis.

References

[1] T. Saito, T. Furuta, T. Yamaguchi, Development of low cost titanium matrix composite, in: F.H. Fries, J. Storer (Eds.), Advances in Titanium Metal Matrix Composites, The Minerals, Metals & Materials Society, Pittsburgh, 1995.

[2] L.J. Huang, L. Geng, H.-X. Peng, Microstructurally inhomogeneous composites: is a homogeneous reinforcement distribution optimal, Prog. Mater. Sci. 71 (2015) 93–168.

[3] K. Morsi, V.V. Patel, Processing and properties of titanium–titanium boride (TiBw) matrix composites - a review, J. Mater. Sci. 42 (2007) 2037–2047.

[4] H. Feng, Y. Zhou, D. Jia, Q. Meng, J. Rao, Growth mechanism of in situ TiB whiskers in spark plasma sintered TiB/Ti metal matrix composites, Cryst. Growth Des. 6 (2006) 1626–1630.

[5] M. Ozerov, M. Klimova, A. Kolesnikov, N. Stepanov, S. Zherebtsov, Deformation behavior and microstructure evolution of a Ti/TiB metal-matrix composite during high-temperature compression tests, Mater. Des. 112 (2016) 17–26.

[6] R. Chaudhari, R. Bauri, A novel functionally gradient Ti/TiB/TiC hybrid composite with wear resistant surface layer, J. Alloys Compd. 744 (2018) 438–444.

[7] R.A. Gaisin, V.M. Imayev, R.M. Imayev, Effect of hot forging on microstructure and mechanical properties of near α titanium alloy/TiB composites produced by casting, J. Alloys Compd. 723 (2017) 385–394.

[8] V. Imayev, R. Gaisin, E. Gaisina, R. Imayev, H.-J. Fecht, Effect of hot forging on microstructure and tensile properties of Ti–TiB, Mater. Sci. Eng. A 609 (2014) 34–41.

[9] C. Leyens, M. Peters, Titanium and Titanium Alloys. Fundamentals and Applications, first ed., Wiley-VCH, Weinheim, 2003.

[10] L. Geng, L. Huang, High temperature properties of discontinuously reinforced titanium matrix composites: a review, Acta Metall. Sin. 27 (2014) 787–797.

[11] L.J. Huang, L. Geng, B. Wang, L.Z. Wu, Effects of volume fraction on the microstructure and tensile properties of in situ TiBw/Ti6Al4V composites with novel network microstructure, Mater. Des. 45 (2013) 532–538.

[12] G.A. Salishchev, S.Yu Mironov, S.V. Zherebtsov, Mechanisms of submicrocrystalline structure formation in titanium and two-phase titanium alloy during warm severe processing, Rev. Adv. Mater. Sci. 11 (2006) 152–158.

[13] G. Will, Powder Diffraction: the Rietveld Method and the Two-Stage Method to Determine and Refine Crystal Structures from Powder Diffraction Data, Springer, Berlin, 2005.

[14] D.B. Williams, C.B. Carter, Transmission Electron Microscopy, Plenum Press, New York, 1996.

[15] M. Ozerov, M. Klimova, A. Vyazmin, N. Stepanov, S. Zherebtsov, Orientation relationship in a Ti/TiB metal-matrix composite, Mater. Lett. 186 (2017) 168–170.

[16] M.Y. Koo, J.S. Park, M.K. Park, K.T. Kim, S.H. Hong, Effect of aspect ratios of in situ formed TiB whiskers on the mechanical properties of TiBw/Ti-6Al-4V composites, Scr. Mater. 66 (2012) 487–490.

[17] S.V. Zherebtsov, G.A. Salishchev, R.M. Galeyev, O.R. Valiakhmetov, S.Yu Mironov, S.L. Semiatin, Production of submicrocrystalline structure in large-scale Ti-6Al-4V billet by warm severe deformation processing, Scripta Mater. 51 (2004) 1147–1151.

[18] S. Zherebtsov, M. Murzinova, G. Salishchev, S.L. Semiatin, Spheroidization of the lamellar microstructure in Ti–6Al–4V alloy during warm deformation and annealing, Acta Mater. 59 (10) (2011) 4138–4150.

[19] S.L. Semiatin, V. Seetharaman, I. Weiss, Flow behavior and globularization kinetics during hot working of Ti-6Al-4V with a colony alpha microstructure, Mater. Sci. Eng. A 263 (2) (1999) 257–271.

[20] F. Humphreys, M. Hatherly, Recrystallization and Related Annealing Phenomena, second ed., Elsevier, Oxford, 2004.

[21] X. Yang, H. Miura, T. Sakai, Grain refinement in magnesium alloy AZ31 during hot deformation, Mater. Sci. Forum 467–470 (2004) 531–536.

[22] O. Sitdikov, T. Sakai, A. Goloborodko, H. Miura, R. Kaibyshev, Grain refinement in coarse-grained 7475 Al alloy during severe hot forging, Phil. Mag. 85 (2005) 1159–1175.

[23] Y.M. Wang, E. Ma, Three strategies to achieve uniform tensile deformation in a nanostructured metal, Acta Mater. 52 (2004) 1699–1709.

[24] S. Zherebtsov, E. Kudryavtsev, S. Kostjuchenko, S. Malysheva, G. Salishchev, Strength and ductility-related properties of ultrafine grained two-phase titanium alloy produced by warm multiaxial forging, Mater. Sci Eng. A 536 (2012) 190–196.

[25] K.S. Munir, Y. Zheng, D. Zhang, J. Lin, Y. Li, C. Wen, Improving the strengthening efficiency of carbon nanotubes in titanium metal matrix composites, Mater. Sci. Eng. A 696 (2017) 10–25.

[26] H. Conrad, Effect of interstitial solutes on the strength and ductility of titanium, Prog. Mater. Sci. 26 (1981) 123–403.

[27] H.J. Frost, M.F. Ashby, Deformation-Mechanism Maps, Pergamon Press, Oxford.

[28] T.M.T. Godfrey, P.S. Goodwin, C.M. Ward-Close, Titanium particulate metal matrix composites—reinforcement, production methods, and mechanical properties, Adv. Eng. Mater. 2 (2000) 85–91.

[29] A.J. Ardell, Precipitation hardening, Metall. Trans. A 16 (12) (1985) 2131–2165.

[30] B. Chen, J. Shen, X. Ye, L. Jia, S. Li, J. Umeda, M. Takahashi, K. Kondoh, Length effect of carbon nanotubes on the strengthening mechanisms in metal matrix composites, Acta Mater. 140 (2017) 317–325.

[31] S. Zherebtsov, M. Ozerov, N. Stepanov, M. Klimova, Yu Ivanisenko, Effect of high-pressure torsion on structure and microhardness of Ti/TiB metal–matrix composite, Metals 7 (2017) 507.